[8] K.A. O'Donnell and E.R. Mendez, J. Opt. Soc. Am. A, 4, 1194 (1987).
[9] M.-J. Kim, J.C. Dainty, A.T. Friborg, and A.J. Sant, J. Opt. Soc. Am. A, 7, 569 (1989).
[10] J.M. Soto-Crespo, M. Nieto-Vesperinas, J. Opt. Soc. Am. A, 6, 376 (1989).
[11] M. Nieto-Vesperinas and J.M. Soto-Crospo, Opt. Lett. 12, 979 (1989).
[12] A. Maradudin, E. Mendex, T. Michel, in Ref. [1].
[13] T.N. Antsygina, V.D. Freilikher, S.A. Gredeskul, L.A. Pastur, V.A. Slusarev, J. of Electromagnetic Waves and Applications, 5, 873 (1991).
[14] V. Freilikher, I. Yurkevich, Physics Letters A, 183, 247 (1993).
[15] V. Freilikher, M. Kaveh, I. Yurkevich, Physica A, 200, 452 (1993).
[16] A. A. Abrikosov and I.A. Ryzkin, Adv. Phys. 27, 146 (1978).
[17] F.G. Bass, I.M. Fuks, "Scattering from Statistically Rough Surface", Pergamon Press, N.Y. (1979).
[18] D. Vollhardt and P. Wölfle, Phys. Rev. B22, 4666 (1980).
[19] V. Freilikher, I. Yurkevich, Physics Letters A, 183, 253 (1993).
[20] S. Feng, A. Arsenieva, Phys. Rev B47, 13047 (1993).
[21] R. Berkovits, M. Kaveh, S. Feng, Phys. Rev. B40, 739 (1989(.
[22] V. Freilikher, M. Pustilnik, I. Yurkevich, Physics Letters A, 193, 467 (1994).
[23] V.D. Freilikher, I.M. Fuks, Izv. Vissh. Uch. Zav., Radiophysics, 13, 98 (1970).
[24] J. Sanchez-Gil, A. Maradudin, J. Lu, V. Freilikher, M. Pustilnik, I. Yurkevich, Phys. Rev. B, 50, 15 353 (1994).
[25] J. Lu, A. Maradudin, T. Michel, J. Opt. Soc. Am. B 8, 311 (1991).
[26] A.R. McGurn and A.A. Maradudin, Optics Comm., 72, 279 (1989).
[27] V. Freilikher, M. Pupstilnik, I. Yurkevich, A. Maradudin, Optics Comm., 110, 63 (1994).

THE INTERACTION OF MICROWAVES WITH SEA ICE

KENNETH M. GOLDEN*

Abstract. The sea ice pack in the polar regions plays a fundamental role in global climate as the boundary layer separating the ocean and atmosphere in these regions. Due to its vast extent, the physical properties of the sea ice pack are often studied via electromagnetic remote sensing from satellites and airplanes, in the microwave regime. In this work we give an overview of ongoing investigations of the interaction of microwaves with sea ice. This interaction is particularly interesting in the case of sea ice, which is a composite of pure ice with random brine and air inclusions, whose geometry can depend dramatically on temperature. These investigations include finding a series of bounds on the effective complex permittivity ϵ^* of sea ice, under constraints on the microgeometry, such as fixed brine volume. In particular, we describe some rather tight bounds on ϵ^* which incorporate the geometrical constraint that for temperatures colder than the percolation threshold, $T_c \approx -5°C$, the brine phase is contained in separated inclusions. These bounds fit actual data on ϵ^* at 4.75 GHz quite closely. We also describe how this series of bounds, which are derived in the quasistatic limit, break down when compared with data taken in the 26.5 - 40.0 GHz range. Finally, we briefly discuss some preliminary results of backscatter experiments we conducted at C band (5.3 GHz) on first year sea ice in the Weddell Sea, Antarctica, during the austral winter of 1994.

Key words. microwaves, complex permittivity, sea ice, matrix-particle composites.

1. Introduction. Sea ice, or frozen sea water, covers 7-10% of the earth's ocean surface. In fact, during the winter the sea ice pack surrounding Antarctica has greater surface area than the continent itself. As the boundary layer separating the ocean and atmosphere in the polar regions, it controls the exchange of heat and momentum between them. In large scale geophysical fluid models, the state of the sea ice pack determines the boundary condition which couples these two fluids. For example, the thickness of the ice helps to determine how well heat is exchanged, and the surface roughness influences the transfer of momentum from, say, the winds to the ocean. Due to the influence of the winds and currents on the motion of the ice, the pack exhibits complex dynamical behavior, which in turn affects the behavior of the atmosphere and ocean. Characterizing the physical state and dynamics of the sea ice pack is a formidable problem. The sheer extent of the pack forces us to turn to remote sensing techniques for recovering large scale information about the pack. In particular, there has been much use of Synthetic Aperture Radar (SAR) sensors mounted on satellites and airplanes, operating in the microwave regime, such as at C band, with frequency $f = 5.3$ GHz and a free space wavelength $\lambda = 5.7$ cm.

The goal of sea ice remote sensing is to use information on the electromagnetic fields returned or scattered by the sea ice to deduce the physical properties of the pack. The electromagnetic properties of sea ice have been

* Department of Mathematics, University of Utah, Salt Lake City, UT 84112, Supported by ONR Grant N000149310141 and NSF Grant DMS-9307324.

studied for a number of years, see for example [1,2,14,16,22,23,24,26,27]. However, the activity in this area has significantly increased recently due to an Accelerated Research Initiative on Sea Ice Electromagnetics from 1992-1997, sponsored by the Office of Naval Research. Over 60 scientists from more than 20 universities and institutes are participating in this program. The scientists include geophysicists, glaciologists, electrical engineers, applied physicists and mathematicians. The program has three major components, consisting of theory, experiments, and field work. The goal of the theoretical work is to develop mathematical models which predict physical properties of the sea ice from reflection or backscatter data. The experimental work is designed to test the models on artificially grown sea ice and identify new phenomena for the models. Most of the experiments have been conducted at the Cold Regions Research and Engineering Laboratory (CRREL) in Hanover, New Hampshire. Field work in the polar regions is being conducted to verify that the theory and experiments correspond to real sea ice.

The mathematical modelling efforts are focused on reconstructing the complex permittivity $\epsilon(x)$ of the sea ice from data on the returned or scattered electric and magnetic fields $E(x,t)$ and $H(x,t)$. Variations in the $\epsilon(x)$ "seen" by the wave are related to the physical properties of sea ice, such as thickness, age, type, snow depth, salinity, roughness, etc. This problem is complicated by the microstructure of sea ice, which is a complex polycrystalline medium of pure ice with random brine and air inclusions. These microstructural variations occur on the millimeter and centimeter scales. For example, in cold first year ice, brine pocket dimensions typically can range from 0.3 mm to 1.5 mm. In the microwave regime, one is typically dealing with free space wavelengths on the order of a few centimeters (although there are windows of higher frequency which exhibit acceptable atmospheric transmission). Consequently, a typical situation, such as at C band, is where the wave *can* resolve variations in $\epsilon(x)$ on the scale $\sim \lambda$ or larger, but the brine and air microstructure on the millimeter scale is averaged out, or "homogenized." In this case, the quasistatic approximation, where the wavelength is much larger than the microstructural scale, is valid. The behavior of the wave inside the sea ice in this case is governed by its effective complex permittivity ϵ^*. In fact, in this regime, the output of inverse algorithms designed to reconstruct the observed permittivity will be a profile of this effective complex permittivity ϵ^*. Currently, such algorithms employing layer stripping, integral equation and other techniques, are being developed by M. Cheney and D. Isaacson (RPI), J. Sylvester and D. Winebrenner (U. of Wash.), and D. Borup, S. Johnson and J. Wiskin (U. of Utah). Since the details of the sea ice microstructure hold the key to characterizing its physical state, such as variation in average brine content, whether it is first year or multiyear ice, its thermal and fluid transport properties, etc., it is important to relate this reconstructed effective permittivity profile to the sea ice microstructure. This is the main focus

of our mathematical work: to understand how the geometry of the brine and air microstructure determines its effective complex permittivity, and in turn, to develop *inverse homogenization* methods to obtain microstructural information from reconstructed effective permittivity data. In fact, a surprisingly accurate method of obtaining inverse bounds on the brine volume of sea ice from complex permittivity data has been developed in [8].

As an example where the wavelength, microstructural, and roughness scales are separated, let us consider the interaction of microwaves at C band with a floe which has a rough surface, say, caused by pressure ridges (and no snow cover). Then backscatter coefficients measured with a mono-static transmitting/receiving microwave horn will be determined primarily by ϵ^* near the surface of the ice, and the statistical behavior of the random surface. In a bi-static configuration, with separate transmitting and receiving horns, the received field at these frequencies will depend primarily on the profile of ϵ^* with depth (in the top layers), as well as the surface roughness. At higher frequencies, in both examples, there will be contributions to the received field from scattering off of the brine and air inclusions.

2. Bounds on the complex permittivity of sea ice by analytic continuation. We are interested in how sea ice microstructure determines the effective electromagnetic behavior of the sea ice. The details of the microstructure, namely the geometry and relative volume fraction of the inclusions, depend strongly on the temperature of the ice, the conditions under which the ice was grown, and the history of the sample under consideration. Due to the wide variety of possible microstructures, and the high dielectric contrast of the components, it is in general quite difficult to accurately predict the effective complex permittivity ϵ^* of sea ice. Nevertheless, many models have been proposed to describe the dielectric behavior of sea ice [1,2,14,16,23,24,26,27]. Typically the sea ice is assumed to consist of a host medium (pure ice) containing spherical or ellipsoidal inclusions (brine or air). Various effective medium theories, such as the coherent potential approximation, have been used to derive "mixing formulas" for the effective permittivity ϵ^* of the system.

While mixing formulas for ϵ^* are certainly useful, their applicability to the full range of microstructures presented by sea ice is limited. For example as sea ice warms up to around $-5°C$, the brine pockets tend to coalesce, or percolate, and form a connected matrix of brine, in which case the sea ice becomes a porous medium. The geometrical assumptions under which most mixing formulas are derived are not satisfied under such circumstances. As we will discuss later, this phase transition has important implications for the overall electromagnetic signature of the sea ice. For example, when the ice is porous, brine and sea water can be transported up through the ice when the floe is weighted down with snow, leaving a

slush layer on top of the ice, which can significantly affect its microwave signature.

Another limitation of mixing formulas is that they provide only a precise prediction of what ϵ^* should be, given, say, a value for the brine volume, yet do not provide any information on the *range* of reasonable values for ϵ^*. In typical experiments one obtains a scatter of data, and it would be useful to compare this spread with a predicted **region** in the complex ϵ^*−plane.

Due to the above limitations in the mixing formula approach which are caused by the wide variety of relevant sea ice microstructures, in recent work we have introduced [12] another approach to studying the effective complex permittivity ϵ^* of sea ice. In particular, we have begun developing a series of bounds on the complex permittivity of the sea ice for given statistical constraints on the brine phase, by applying an analytic method for obtaining bounds on the effective properties of composite materials [4,20,13]. In this method, the sea ice is assumed to be a two-component random medium consisting of brine of permittivity ϵ_1, and ice of permittivity ϵ_2. The method exploits the properties of ϵ^* as an analytic function of the ratio ϵ_1/ϵ_2. The key step in the method is to obtain an integral representation for ϵ^*, which is exploited to obtain the bounds. As in the case of typical mixing formulas, the bounds are derived in the quasistatic limit, so that they are valid when the wavelength is long compared to the scale of the inhomogeneities.

In order to describe the series of bounds we have been developing, let us briefly review the analytic continuation method for studying the effective properties of composite materials. For simplicity we consider a random medium in all of R^d. Let $\epsilon(x,\omega)$ be a (spatially) stationary random field in $x \in R^d$ and $\omega \in \Omega$, where Ω is the set of all realizations of our random medium. We assume $\epsilon(x,\omega)$ takes the values ϵ_1 and ϵ_2, which are complex numbers, and write

$$\epsilon(x,\omega) = \epsilon_1\chi_1(x,\omega) + \epsilon_2\chi_2(x,\omega), \tag{2.1}$$

where χ_j is the characteristic function of medium $j = 1,2$, which equals one for all realizations $\omega \in \Omega$ having medium j at x, and equals zero otherwise. Let $E(x,\omega)$ and $D(x,\omega)$ be the stationary random electric and displacement fields satisfying

$$D(x,\omega) = \epsilon(x,\omega)E(x,\omega) \tag{2.2}$$

$$\nabla \cdot D(x,\omega) = 0 \tag{2.3}$$

$$\nabla \times E(x,\omega) = 0 \tag{2.4}$$

$$< E(x,\omega) >= e_k, \tag{2.5}$$

where e_k is a unit vector in the k^{th} direction, for some $k = 1,\ldots,d$, and $< \cdot >$ means ensemble average over Ω or spatial average over all of R^d.

In view of the local constitutive law (2.2), the effective complex permittivity tensor ϵ^* is defined as

$$< D >= \epsilon^* < E > . \tag{2.6}$$

For simplicity, we focus on one diagonal coefficient $\epsilon^* = \epsilon^*_{kk}$. Due to the homogeneity of effective parameters, $\epsilon^*(\lambda\epsilon_1,\lambda\epsilon_2) = \lambda\epsilon^*(\epsilon_1,\epsilon_2)$, ϵ^* depends only on the ratio $h = \frac{\epsilon_1}{\epsilon_2}$, and we define $m(h) = \frac{\epsilon^*}{\epsilon_2}$. The two main properties of $m(h)$ are that it is analytic off $(-\infty,0]$ in the h−plane, and that it maps the upper half plane to the upper half plane [3,13], so that it is an example of a Herglotz, or Stieltjes function.

As mentioned above, the key step in the analytic continuation method is obtaining an integral representation for ϵ^*. For this purpose it is more convenient to look at the function [3]

$$F(s) = 1 - m(h) = 1 - \frac{\epsilon^*}{\epsilon_2}, \quad s = 1/(1-h), \quad h = \frac{\epsilon_1}{\epsilon_2}, \tag{2.7}$$

which is analytic off $[0,1]$ in the s−plane. It was then proven in [13] that $F(s)$ has the following representation

$$F(s) = \int_0^1 \frac{d\mu(z)}{s-z}, \qquad s \notin [0,1], \tag{2.8}$$

where μ is a positive measure on $[0,1]$. One of the most important features of (2.8) is that it separates the parameter information in $s = 1/(1-\epsilon_1/\epsilon_2)$ from information about the geometry of the mixture, which is all contained in μ. Actually, μ is the spectral measure associated with the operator $\Gamma\chi_1$, where $\Gamma = \nabla(-\Delta)^{-1}\nabla\cdot$, and χ_1 is the characteristic function of medium 1, equaling 1 in medium 1 and 0 otherwise, which determines the geometry.

Statistical assumptions about the geometry are incorporated into μ through its moments

$$\mu_n = \int_0^1 z^n d\mu(z). \tag{2.9}$$

Comparison of a perturbation expansion of (2.8) around a homogeneous medium ($s = \infty$, or $\epsilon_1 = \epsilon_2$) with a similar expansion of a resolvent representation for $F(s)$ [13], yields

$$\mu_n = (-1)^n < \chi_1[(\Gamma\chi_1)^n e_k] \cdot e_k > . \tag{2.10}$$

Then

$$\mu_0 = p_1 \tag{2.11}$$

if only the volume fractions are known, and

$$\mu_1 = \frac{p_1 p_2}{d} \tag{2.12}$$

if the material is statistically isotropic, where d is the dimension of the system. In general, knowledge of the $(n+1)$-point correlation function of the medium allows calculation of μ_n (in principle).

Bounds on ϵ^*, or $F(s)$, are obtained by fixing s in (2.8), varying over admissible measures μ (or admissible geometries), such as those that satisfy only (2.11), and finding the corresponding range of values of $F(s)$ in the complex plane. Two types of bounds on ϵ^* are obtained. The first bound R_1 assumes only that the relative volume fractions p_1 and $p_2 = 1 - p_1$ of the brine and ice are known, so that (2.11) is satisfied. In this case, the admissible set of measures forms a compact, convex set. Since (2.8) is a linear functional of μ, the extreme values of F are attained by extreme points of the set of admissible measures, which are the Dirac point measures of the form $p_1\delta_z$. The values of F must lie inside the circle $p_1/(s-z)$, $-\infty \leq z \leq \infty$, and the region R_1 is bounded by circular arcs, one of which is parametrized in the F-plane by

$$C_1(z) = \frac{p_1}{s-z}, \qquad 0 \leq z \leq p_2. \tag{2.13}$$

To display the other arc, it is convenient to use the auxiliary function [5]

$$E(s) = 1 - \frac{\epsilon_1}{\epsilon^*} = \frac{1 - sF(s)}{s(1-F(s))}, \tag{2.14}$$

which is a Herglotz function like $F(s)$, analytic off $[0,1]$. Then in the E-plane, we can parametrize the other circular boundary of R_1 by

$$\hat{C}_1(z) = \frac{p_2}{s-z}, \qquad 0 \leq z \leq p_1. \tag{2.15}$$

In the ϵ^*-plane, R_1 has vertices $V_1 = \epsilon_1/(1-\hat{C}_1(0)) = (p_1/\epsilon_1 + p_2/\epsilon_2)^{-1}$ and $W_1 = \epsilon_2(1 - C_1(0)) = p_1\epsilon_1 + p_2\epsilon_2$, and collapses to the interval

$$(p_1/\epsilon_1 + p_2/\epsilon_2)^{-1} \leq \epsilon^* \leq p_1\epsilon_1 + p_2\epsilon_2 \tag{2.16}$$

when ϵ_1 and ϵ_2 are real, which are the classical arithmetic (upper) and harmonic (lower) mean bounds, also called the elementary bounds. The complex elementary bounds (2.13) and (2.15) are optimal and can be attained by a composite of uniformly aligned spheroids of material 1 in all sizes coated with confocal shells of material 2, and vice versa. These arcs are traced out as the aspect ratio varies.

If the material is further assumed to be statistically isotropic, i.e., $\epsilon^*_{ik} = \epsilon^*\delta_{ik}$, then (2.12) must be satisfied as well. A convenient way of including this information is to use the following transformation [5,11],

$$F_1(s) = \frac{1}{p_1} - \frac{1}{sF(s)}. \tag{2.17}$$

The function $F_1(s)$ is, again, a Herglotz function which has the representation

$$F_1(s) = \int_0^1 \frac{d\mu^1(z)}{s-z}. \tag{2.18}$$

The constraint (2.12) on $F(s)$ is then transformed to a restriction of only the mass, or zeroth moment μ_0^1 of μ^1, with

$$\mu_0^1 = p_2/p_1 d. \tag{2.19}$$

Applying the same procedure as for R_1 yields a region R_2, whose boundaries are again circular arcs. In the F-plane, one of these arcs is parametrized by

$$C_2(z) = \frac{p_1(s-z)}{s(s-z-p_2/d)}, \qquad 0 \leq z \leq (d-1)/d. \tag{2.20}$$

(We point out that in eq. (25) in [12] and eq. (2.20) in [21], there is a p_1 in the denominator which should be a p_2, as above.) In the E-plane, the other arc is parametrized by

$$\hat{C}_2(z) = \frac{p_2(s-z)}{s(s-z-p_1(d-1)/d)}, \qquad 0 \leq z \leq 1/d. \tag{2.21}$$

In the ϵ^*-plane, R_2 has vertices $V_2 = \epsilon_2(1-C_2(0))$ and $W_2 = \epsilon_1/(1-\hat{C}_2(0))$, and collapses to the interval

$$\epsilon_2 + p_1 \Big/ \left(\frac{1}{\epsilon_1 - \epsilon_2} + \frac{p_2}{d\epsilon_2}\right) \leq \epsilon^* \leq \epsilon_1 + p_2 \Big/ \left(\frac{1}{\epsilon_2 - \epsilon_1} + \frac{p_1}{d\epsilon_1}\right), \tag{2.22}$$

when ϵ_1 and ϵ_2 are real with $\epsilon_1 \geq \epsilon_2$, which are the Hashin–Shtrikman bounds [15]. When $\epsilon_1 \leq \epsilon_2$, the sequence of inequalities is reversed. The vertices V_2 and W_2 (which correspond to the expressions in (2.22)), are attained by the Hashin–Shtrikman coated sphere geometries (spheres of all sizes of material 1 in the volume fraction p_1 coated with spherical shells of material 2 in the volume fraction p_2, and vice versa), and lie on the arcs which bound R_1. We remark that higher-order correlation information can be conveniently incorporated by iterating (2.17), as in [11].

To summarize, R_1 is a region in the complex ϵ^*-plane, bounded by circular arcs, in which ϵ^* for any microgeometry with the given volume fractions must lie. In addition to the volume fractions, the second region R_2 assumes that the composite is statistically isotropic, is again bounded by circular arcs, and lies inside R_1. These bounds are compared in [12] with the experimental data of Arcone, Gow and McGrew [2] for artificially grown sea ice at 4.75 and 9.5 GHz. Given a sample of sea ice at temperature T

degrees Celsius and of salinity S parts per thousand (ppt), we estimate the relative brine volume p_1 using the equation of Frankenstein and Garner [10],

$$p_1 = \frac{S}{1000}\left(\frac{49.185}{|T|} + 0.532\right). \tag{2.23}$$

Then for each frequency, 4.75 and 9.5 GHz, and for a given temperature T, we find the complex permittivity of the brine ϵ_1 using the calculations of Stogryn and Desargant [25], which are based on a Debye-type relaxation equation,

$$\epsilon_1 = \epsilon_\infty + \frac{\epsilon_s - \epsilon_\infty}{1 - i2\pi f\tau} + i\frac{\sigma}{2\pi\epsilon_0 f}, \tag{2.24}$$

which has only one resonance, ignoring a possible spread in relaxation times. In (2.24), ϵ_s and ϵ_∞ are the limiting static and high frequency values of the real part of ϵ_1, τ is the relaxation time, f is the frequency, σ is the ionic conductivity of the dissolved salts, ϵ_0 is the permittivity of free space, and $i = \sqrt{-1}$. The ionic conductivity is assumed to be independent of frequency. Then ϵ_1 for brine in equilibrium with sea ice is determined by the four real parameters $\epsilon_\infty, \epsilon_s, \tau$ and σ, each of which depends only on temperature, and were found experimentally. Also, in the experiments, only vertically incident waves were considered. While the brine inclusions tend to be elongated in the vertical direction, they form a statistically isotropic structure within the horizontal plane (except when there is a well defined current direction during growth, which can cause marked anisotropy in ϵ^* [14]). We are therefore justified in employing bounds based on (2.12), and because of the geometry we take $d = 2$. Finally, in work done subsequent to [12], we have found [8] that the theoretical bounds fit the data more closely if one accounts for the air in the sea ice. In particular, we slightly adjust the complex permittivity ϵ_2 of the ice by treating it as a composite with a small volume fraction of air, and calculating its effective permittivity ϵ_2 with the Maxwell–Garnett formula,

$$\epsilon_2 = \epsilon_{ice}\left[1 - \frac{d\,p_{air}(\epsilon_{ice} - \epsilon_{air})}{\epsilon_{ice}(d-1) + \epsilon_{air} + p_{air}(\epsilon_{ice} - \epsilon_{air})}\right], \tag{2.25}$$

where $\epsilon_{ice} = (3.1884 + 0.00091\,T) + i\,0.00005$ [19], $\epsilon_{air} = 1$, and p_{air}, the volume fraction of air, is calculated according to the equations in [9], which depend on the density of the of the sea ice sample, T and S. In (2.25) we take $d = 3$, as the air inclusions in the actual sea ice are uniformly and isotropically distributed throughout the ice in three dimensions (as opposed to the brine). We remark that (2.25) should give a quite good estimate of the effective permittivity of the ice, as p_{air} is small, and more importantly, the contrast between ϵ_{ice} and ϵ_{air} is quite small (at least in comparison to the contrast between ϵ_1 and ϵ_2).

In general, we have obtained excellent agreement in comparing the bounds with the data, particularly now that we have included the effect of the air. However, in the next section we will describe an even tighter set of bounds which again correlate very well with the data, and it is in that section where will display a figure showing the full series of bounds compared with a representative data set.

3. Improved bounds on the complex permittivity of sea ice as a matrix-particle composite. In [12], a striking feature of the figures illustrating the comparison of the experimental data with the bounds R_1 and R_2 is that the data consistently lie in the lower portion of the bounds, i.e., where $Re(\epsilon^*)$ and $Im(\epsilon^*)$ are small in comparison to the whole regions. This observation suggests that the ice phase is dominating the behavior, which reflects the microstructural feature that the brine is contained in inclusions, and does not form a connected matrix, or percolate. For "cold" sea ice, this is certainly a reasonable assumption about the geometry. However, when the temperature of the sea ice is near the critical temperature $T_c \approx -5°C$, this assumption breaks down. In order to try and capture the data in [2] more closely, we have incorporated the non-percolation assumption about the brine phase into our series of bounds, by turning to the work of Bruno [6]. In this seminal paper, Bruno has found restrictions on the support of μ in the integral representation (2.8) which arise from imposing the geometrical condition that one phase is contained in separated inclusions embedded in a matrix of the other material. The further the separation, the tighter the restriction on the support. Based on this support restriction, Bruno has derived bounds on the effective conductivity, in the case of real component conductivities, of some matrix-particle composites. In [21], Sawicz and Golden have extended these bounds to the complex case, and applied them to the sea ice data considered in [12]. Unfortunately, we must alert the reader that there are some errors in the figures and in one of the equations in [21] (as well as some typographical errors), which this author has only recently discovered, and which are corrected here. One of the reasons for developing bounds based on the matrix-particle assumption is that more general bounds begin to break down, and become trivial in the high contrast limit. For example, as $\epsilon_1 \to \infty$ in (2.22), the upper Hashin-Shtrikman bound diverges. For composites made of highly contrasting components, such as the ice and brine of sea ice, such bounds which do not become trivial are clearly of significant use.

To describe the new complex bounds, we must first briefly review [6,7] the main ideas of Bruno's work on how the matrix-particle assumption restricts the support of the measure μ. While the general, stationary random formulation of the effective permittivity problem given in the previous section is still valid, it is perhaps more useful at this point, given that we are considering a specific class of possible geometries, to focus on this spatial dependence.

Let us consider a material occupying a cubic (or square) box Λ in R^d,with $0 \leq x_i \leq 1$, $1 \leq i \leq d$. We assume that the material consists of a matrix of permittivity ϵ_2 containing a finite, arbitrarily large number of non-touching grains of permittivity ϵ_1. The region of Λ occupied by ϵ_2 will be referred to as the outside region, denoted by Λ^{out}, and the inside region containing ϵ_1 is denoted by Λ^{in}. We assume that Λ is very large compared to the microstructural scale, which is determined by the size and spacing of the inclusions. The local permittivity $\epsilon(x)$ is still given by (2.1). For simplicity, the inclusions are assumed to be connected regions with smooth boundaries. However, all results hold for grain shapes with boundaries of Lipschitz type as well, which include those with certain types of singularities, such as polygons and polyhedra with corners and edges. If the upper and lower faces of Λ are kept at constant potentials $\Phi(x_d = 1) = 1$ and $\Phi(x_d = 0) = 0$, the electric potential Φ inside the box Λ satisfies

$$\nabla \cdot (\epsilon \nabla \Phi) = 0, \tag{3.1}$$

with the boundary condition $\frac{\partial \Phi}{\partial n} = 0$ along the vertical walls, as well as the equipotential condition on the top and bottom faces. The effective permittivity is then defined by

$$\epsilon^* = \int_\Lambda \epsilon \frac{\partial \Phi}{\partial x_d} \, dV, \tag{3.2}$$

or equivalently by

$$\epsilon^* = \int_\Lambda \epsilon \, |\nabla \Phi|^2 \, dV. \tag{3.3}$$

Correspondence with the previous section is obtained by taking the limit as the microstructural scale $\to 0$, or as the volume becomes infinite, with appropriate normalization in (3.2) and (3.3). See [13], for example. Again it will be important to consider the functions

$$m(h) = \frac{\epsilon^*}{\epsilon_2}, \qquad h = \frac{\epsilon_1}{\epsilon_2} \tag{3.4}$$

and

$$F(s) = 1 - m(h), \qquad s = \frac{1}{1-h}. \tag{3.5}$$

Recall that general arguments alone yield only that $m(h)$ is analytic off $(-\infty, 0]$ in the $h-$plane, while $F(s)$ is analytic off $[0, 1]$ in the $s-$plane. Note that Φ is harmonic in Λ^{out} and Λ^{in}, i.e.,

$$\Delta \Phi^{in} = \Delta \Phi^{out} = 0. \tag{3.6}$$

Across the boundary γ separating Λ^{out} and Λ^{in}, Φ must be continuous, and yield continuity of the normal component of $D = \epsilon E$.

Now, the physical observation which underlies the restriction of the spectral measure is that in high contrast media with inclusions, energy is concentrated where the inclusions begin to touch. If these situations can be avoided, then the energy can be controlled. In particular, if we consider a class of media *defined* in terms of control on the energy, then one can obtain the estimates necessary to get convergence of a series which allows further analytic continuation of $m(h)$ or $F(s)$ beyond the domains given in the previous section. Thus we make the following assumptions about the matrix-particle array under consideration. For each inclusion I, we assume that there is a connected region I' containing I, again with a smooth (or Lipschitz) boundary, and such that $I - I'$ is a connected subset of Λ, in such a way that for certain positive constants A and B we have the following:

1. For any inclusion I, the region I' is contained in Λ.
2. If I and J are two different inclusions, then I' and J' do not intersect.
3. For each inclusion I and for any function $u' \in H^1(I' - I)$ there exists a function $u \in H^1(I' - I)$ satisfying

$$u(x) = u'(x), \qquad x \in I' - I \tag{3.7}$$

and

$$\int_I |\nabla u|^2 dV \leq A \int_{I'-I} |\nabla u'|^2 dV. \tag{3.8}$$

4. For each inclusion I and for any function $u \in H^1(I)$ there exists a function $u' \in H^1(I' - I)$ such that u' vanishes on the boundary of I', its boundary values at the boundary of I differ from those of u by a constant, and one has

$$\int_{I'-I} |\nabla u'|^2 dV \leq B \int_I |\nabla u|^2 dV. \tag{3.9}$$

A material which satisfies all of these assumptions is referred to as a material of type $C_{A,B}$. It can be shown that for any two regions I and I' as above, there always exist constants A and B such that (3) and (4) above are satisfied. We remark that the idea of using extensions of potentials which preserve energy estimates was first introduced by Tartar in proving homogenization for certain systems with "hard" inclusions. Materials of type $C_{A,B}$ enjoy the following global properties:

Property C_A : For every function $u^{out} \in H^1(\Lambda^{out})$, there exists a function $u \in H^1(\Lambda)$ which coincides with u^{out} in the region Λ^{out}, and which satisfies the inequality

$$\int_{\Lambda^{in}} |\nabla u|^2 \, dV \leq A \int_{\Lambda^{out}} |\nabla u^{out}|^2 \, dV. \tag{3.10}$$

Property C_B : For every function $u^{in} \in H^1(\Lambda^{in})$, there exists a function $u \in H^1(\Lambda^{out})$ such that, its restriction to the boundary of any grain differs by a constant from the restriction of u^{in} to the boundary of that grain (the constants may differ from grain to grain), it vanishes outside the union of all I's, and such that

$$\int_{\Lambda^{out}} |\nabla u|^2 \, dV \leq B \int_{\Lambda^{in}} |\nabla u^{in}|^2 \, dV. \tag{3.11}$$

For materials satisfying the above properties, we have the following main results [6].

THEOREM 3.1. *For a material satisfying property* C_A, *the potential* $\Phi(x,h)$ *and the (normalized) effective permittivity* $m(h)$ *can be analytically continued to the disk* $|h| < \frac{1}{A}$.

THEOREM 3.2. *For a material satisfying property* C_B, *the potential* $\Psi(x,w) = \Phi(x,1/h)$ *and the (normalized) effective permittivity* $m(w), w = \frac{1}{h}$ *can be analytically continued to the disk* $|w| < \frac{1}{B}$.

THEOREM 3.3. *For a material satisfying properties* C_A *and* C_B, *the (normalized) effective permittivity* $m(h)$ *is analytic off the interval* $[-B, -\frac{1}{A}]$ *in the* $h-$*plane.*

We remark that the main idea used in establishing, say, Theorem 3.1, is to obtain convergence of the expansion

$$\Phi(x,h) = \sum_{i=0}^{\infty} \Phi_i(x) \, h^i. \tag{3.12}$$

The key tool is to use Property C_A to obtain the estimate

$$\int_{\Lambda} |\Phi_i|^2 \, dV \leq CA^{2i} \int_{\Lambda} |\nabla \Phi_0|^2 \, dV, \tag{3.13}$$

so that the mean square norm of Φ_i is bounded by a constant times A^i, which leads to the result.

As a consequence of Theorem 3.3, the support of the measure μ in the integral representation (2.8) for $F(s)$ is contained in the interval

$$s_m \leq s \leq s_M, \tag{3.14}$$

$[s_m, s_M] \subset [0,1]$, where

$$s_m = \frac{1}{1+B}, \quad s_M = \frac{A}{A+1}. \tag{3.15}$$

Then (2.8) takes the form

$$F(s) = \int_{s_m}^{s_M} \frac{d\mu(z)}{s-z}. \tag{3.16}$$

To obtain complex bounds on ϵ^* which incorporate the matrix-particle assumption for type $C_{A,B}$ materials, we exploit the restricted representation (3.16), for given values of s_m and s_M. We will describe later how these values are chosen for relevant sea ice microgeometries. As indicated in (2.11), if one assumes that the relative volume fractions of the two constituents are known, then the mass μ_0 of μ satisfies $\mu_0 = p_1$. If one further assumes that the microgeometry is statistically isotropic, then (2.12) also holds. For $C_{A,B}$ materials these constraints must be combined with the support restriction on μ reflected in (3.16). A convenient way of incorporating the support restriction is to first consider a new variable t, defined by

$$s = (s_M - s_m)t + s_m. \tag{3.17}$$

Then the interval $[s_m, s_M]$ in the $s-$plane gets mapped to $[0,1]$ in the $t-$plane, and the function

$$H(t) = F(s) = F((s_M - s_m)t + s_m) \tag{3.18}$$

is analytic off $[0,1]$ in the complex $t-$plane. It can be shown that there is a positive Borel measure ν on $[0,1]$ such that

$$H(t) = \int_0^1 \frac{d\nu(z)}{t-z}. \tag{3.19}$$

Letting

$$\lambda = s_M - s_m \tag{3.20}$$

be the spectral width, it can be shown using (2.11) and (2.12) that

$$\nu_0 = \frac{p_1}{\lambda} \tag{3.21}$$

if only the volume fractions are known, and

$$\nu_1 = \frac{p_1}{\lambda^2}\left(\frac{p_2}{d} - s_m\right) \tag{3.22}$$

if the material is statistically isotropic.

Now let us assume only that (3.21) is satisfied, and we apply the same extremal procedure described above to see that the values of H lie inside the circle

$$K_1(z) = \frac{p_1/\lambda}{t-z}, \qquad -\infty \leq z \leq \infty. \tag{3.23}$$

In the $F-$plane this translates via (3.17) and (3.18) into the circle

$$K_1'(z) = \frac{p_1}{s - (\lambda z + s_m)}, \qquad -\infty \leq z \leq \infty, \tag{3.24}$$

which happens to coincide with the circle $C_1(z)$, $-\infty \le z \le \infty$, so that the matrix-particle assumption in this case provides no improvement over the standard complex elementary bound. Now we consider the analog $G(t)$ of $E(s)$ defined by

$$G(t) = \frac{1 - tH(t)}{t(1 - H(t))}. \tag{3.25}$$

Then $G(t)$ has an integral representation

$$G(t) = \int_0^1 \frac{d\rho(z)}{t - z}, \tag{3.26}$$

where the mass of ρ is

$$\rho_0 = 1 - \frac{p_1}{\lambda}. \tag{3.27}$$

We then obtain a circle in the $G-$plane analogous to $\hat{C}_1(z)$ in (2.15),

$$\hat{K}_1(z) = \frac{1 - p_1/\lambda}{t - z}, \qquad -\infty \le z \le \infty. \tag{3.28}$$

In the $F-$plane this becomes via (3.25) and (3.18)

$$\hat{K}_1'(z) = \frac{p_1(s - s_m) - \lambda^2 z}{(s - s_m)(p_1 - \lambda + s - s_m) - \lambda^2 z}, \quad -\infty \le z \le \infty, \tag{3.29}$$

which is an improvement over (2.15). Back in the ϵ^*-plane, the intersection of the two circles (3.24) and (3.29) yields a region R_1^{mp} which has vertices $V_1^{mp} = \epsilon_2(1 - \hat{K}_1'(0))$ and $W_1^{mp} = \epsilon_2(1 - K_1'(0))$. When ϵ_1 and ϵ_2 are real and positive, R_1^{mp} collapses to the interval with endpoints V_1^{mp} and W_1^{mp},

$$\epsilon_2 \frac{\epsilon_2 - s_M(\epsilon_2 - \epsilon_1)}{\epsilon_2 - (s_M - p_1)(\epsilon_2 - \epsilon_1)} \le \epsilon^* \le \epsilon_2 \frac{\epsilon_2 - (s_m + p_1)(\epsilon_2 - \epsilon_1)}{\epsilon_2 - s_m(\epsilon_2 - \epsilon_1)}. \tag{3.30}$$

These bounds are tighter than the classical arithmetic and harmonic mean bounds and reduce to them for $s_m = 0$ and $s_M = 1$. (Eq. (3.34) in [21] is an incorrect version of (3.29), and the corresponding region in Figure 2 in [21] is incorrect as well.)

Finally, we consider the case where the material is further assumed to be statistically isotropic. Let

$$H_1(t) = \frac{1}{\nu_0} - \frac{1}{tH(t)} = \frac{\lambda}{p_1} - \frac{1}{tH(t)}. \tag{3.31}$$

Then H_1 is a Herglotz function which is analytic off $[0, 1]$ and has an integral representation in terms of a measure ν^1, which can be shown to have mass

$$\nu_0^1 = \frac{\nu_1}{(\nu_0)^2} = \frac{\frac{p_2}{d} - s_m}{p_1}. \tag{3.32}$$

Then the allowed values of $H_1(t)$ are contained inside the circle $\nu_0^1/(t - z)$, $-\infty \le z \le \infty$, which becomes in the $H-$plane

$$K_2(z) = \frac{\nu_0^2(t - z)}{t(\nu_0(t - z) - \nu_1)}, \qquad -\infty \le z \le \infty, \tag{3.33}$$

or in the $F-$plane,

$$K_2'(z) = \frac{p_1(s - s_m - z\lambda)}{(s - s_m)(s - p_2/d - z\lambda)}, \qquad -\infty \le z \le \infty. \tag{3.34}$$

For $s_m = 0$ and $s_M = 1$ ($\lambda = 1$) the above circle is identical with the full circle containing the arc (2.20).

To obtain the other circle, we apply a similar transformation to $G(t)$, obtaining a function

$$G_1(t) = \frac{1}{\rho_0} - \frac{1}{tH(t)} = \frac{\lambda}{\lambda - p_1} - \frac{1}{tH(t)}, \tag{3.35}$$

which, again, is a Herglotz function analytic off $[0, 1]$ with representing measure ρ^1 of mass

$$\rho_0^1 = \frac{\nu_0(1 - \nu_0) - \nu_1}{(1 - \nu_0)^2}. \tag{3.36}$$

Then in the G_1-plane, the allowed values are contained inside the circle $\rho_0^1/(t - z)$, $-\infty \le z \le \infty$, which becomes in the $G-$plane

$$\hat{K}_2(z) = \frac{(1 - \nu_0)(t - z)}{t(t - z - \nu_0 + \nu_1/(1 - \nu_0))}, \quad -\infty \le z \le \infty. \tag{3.37}$$

The intersection of the two circles (3.34) and (3.37) (in a common plane) yields a region R_2^{mp} which in the ϵ^*- plane has vertices $V_2^{mp} = \epsilon_2(1 - K_2'(0))$ and W_2^{mp}, which is the image of $\hat{K}_2(0)$ in the ϵ^*- plane. The region R_2^{mp} is an improvement over the complex Hashin-Shtrikman bounds under the matrix-particle assumption. When ϵ_1 and ϵ_2 are real and positive, with $\epsilon_1 \ge \epsilon_2$, R_2^{mp} collapses to the interval with endpoints V_2^{mp} and W_2^{mp},

$$1 - \frac{p_1}{s - p_2/d} \le \frac{\epsilon^*}{\epsilon_2} \le \frac{s - s_M}{s - s_m}\left(1 + \frac{1 - \nu_0^2}{(1 - \nu_0)t + \nu_1}\right). \tag{3.38}$$

Note that the left endpoint V_2^{mp} is the lower Hashin-Shtrikman expression, so that it coincides with the same vertex from the region R_2. When $\epsilon_1 \le \epsilon_2$ the sequence of inequalities is reversed. (We point out that in eqs. (3.44) and (3.47) in [21], which correspond to (3.38) here, there is a typographical error that also appeared in [6]. Furthermore, the inner regions R_2^{mp} of figures 3 and 4 in [21] have been plotted incorrectly.) Finally, we note

that the positivity of the moments of the measures ν and ρ imply that the spectrum cannot be too small [6],

$$s_m \leq p_2/d\,, \quad s_M \geq p_2/d + p_1\,. \tag{3.39}$$

In the previous section it was described how we obtain p_1, ϵ_1 and ϵ_2 for given sea ice samples in order to compare the permittivity data in [2] with our bounds. For our two dimensional sea ice geometry, in order to compare with the matrix-particle bounds, we further assume that the brine is contained in circular discs, which allows us to utilize the explicit calculations in [6] of the constants A and B, as well as s_m and s_M. Our class of materials then is as follows. Discs of brine of radius r_b hold random positions in a host of ice, in such a way that each disc of brine is surrounded by a "corona" of ice, with outer radius r_i. Then the minimal separation of brine inclusions is $2(r_i - r_b)$. Such a medium is called a $q-$material, where $q = r_b/r_i$. For such a geometry, Bruno has calculated [6]

$$s_m = \frac{1}{2}(1-q^2), \quad s_M = \frac{1}{2}(1+q^2). \tag{3.40}$$

Smaller q values indicate well separated brine (and presumably cold temperatures), and $q = 1$ corresponds to $s_m = 0, s_M = 1$, in which case R_1^{mp} and R_2^{mp} reduce to R_1 and R_2. Examination of photomicrographs of the brine microstructure in the sea ice samples of [2] indicates that even when the ice is quite cold, and well above its percolation threshold, the brine inclusions are quite close, and it is very difficult to estimate appropriate values of q. Instead, for a given data set at a particular temperature, we choose a value of q which best captures the data, and it is always quite close to 1. (Computationally we find that because of the high contrast in the components, the bounds R_1^{mp} and R_2^{mp} are extremely sensitive to small changes in q for q near 1.) By very carefully comparing our bounds to data over a wide range of temperatures, we have found that the appropriate q value does indeed approach 1 as the temperature progresses through the percolation threshold. In fact, we have found that as the temperature increases, i.e. as the percolation threshold is approached, the data sweeps across from one side of the region R_2 to the other (while R_2 becomes larger as the brine volume increases), following an arc of R_2^{mp}. Once the temperature is above T_c, the data require that $q = 1$, and the matrix-particle assumption is no longer valid. These findings will be detailed elsewhere. A typical example of the comparison of the data in [2] with the bounds R_1, R_2, R_1^{mp} and R_2^{mp} is shown in Fig. 1.

4. Microwave experiments on sea ice. In addition to our theoretical work on bounding the effective complex permittivity ϵ^* of sea ice, we are also interested in microwave experiments designed to investigate its electromagnetic properties. We now briefly describe these experiments, and some of the preliminary findings.

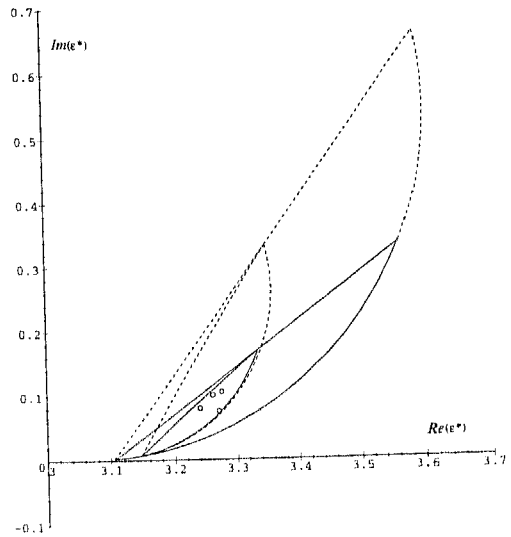

FIG. 1. *Comparison of experimental data (circles) on ϵ^* with bounds R_1 (outer, dotted), R_2 (inner, dotted), R_1^{mp} (outer, solid), and R_2^{mp} (inner, solid). R_1 assumes only knowledge of the brine volume and R_2 assumes statistical isotropy as well. R_1^{mp} and R_2^{mp} further assume that the sea ice is a matrix-particle composite with $q = 0.97$. For the data, the frequency $f = 4.75$ GHz, salinity $S = 3.8$ ppt, temperature $T = -14°C$, and the brine volume $p_1 = 0.015$. The complex permittivities of the brine and ice are $\epsilon_1 = 38.26 + i43.99$ and $\epsilon_2 = 3.06$ (with a 0.041 volume fraction of air in the ice).*

Our theoretical bounds on ϵ^* for sea ice have been compared with the experimental data taken by Arcone, Gow and McGrew [2] for artificially grown sea ice at 4.8 and 9.5 GHz, where the quasistatic approximation is certainly valid, and excellent agreement was obtained. Recently, though, S. Ackley and V. I. Lytle have made measurements of ϵ^* on cores cut from "sea ice" which was artificially grown in the cement pond at CRREL. By measuring the travel time and attenuation of a pulse as it travels down through the axis of a vertically drilled, cylindrical core, they can find the real and imaginary parts of ϵ^*. What is particularly interesting about their measurements is that they were done using microwave pulses at Ka band, with a bandwidth of 26.5 - 40.0 GHz, where the validity of the quasi-static approximation is uncertain. In fact, at these frequencies, the wavelength in the medium is on the order of 4 mm, while the typical brine pocket dimension in the direction perpendicular to the propagation is on the order of 1 or 2 mm, so that the wavelength is larger, but certainly on the same order as the microstructural scale. In further experiments, cores have been cut horizontally through the ice so that the electric field can sample the long, vertical dimension of the brine pockets.

We have compared some of the data with the fixed brine volume bounds, and found that the data often lie significantly outside the region R_1. Apparently in this frequency range we are beginning to see scattering

effects with the breakdown of the quasistatic approximation. Currently we are looking at extrapolations of this data to lower frequencies using the strong fluctuation theory of T. Grenfell and S. Nghiem in order to compare this new data with our bounds.

In addition to the above comparison of theoretical and laboratory work, Ackley, Lytle and Golden have collaborated on sea ice field experiments as members of a cruise aboard the NSF Research Vessel N.B. Palmer to the Weddell Sea, Antarctica, during July and August of 1994. The cruise formed a core component of the Antarctic Zone Flux (ANZFLUX) Program, which was designed to measure vertical fluxes of heat, salt, and momentum in the eastern Weddell Gyre. Part of the motivation for the program was a lack of understanding of vertical oceanic heat fluxes, or upwelling, in this area, believed responsible for the so-called "Weddell polynya," or large "hole" in the sea ice pack which persisted during a series of winter seasons in the early 1970's. An essential component of the cruise was to characterize the physical properties of the sea ice pack associated with observed atmospheric and oceanic conditions and events.

In conjunction with this work, Lytle and Golden conducted microwave backscatter experiments on the primarily first year sea ice present in the region [18]. We used a C band, transmitting and receiving radar apparatus, with a center frequency of 5.3 Ghz, and a 500 MHz bandwidth. The radar employs a Frequency Modulated Continuous Wave (FMCW), which is transmitted by a parabolic dish and is received by one of two microwave horns, depending on desired polarization, all of which is mounted on one platform, so that the radar operates in a mono-static, or backscatter mode. The radar was mounted on the bridge of the ship.

We are interested in correlating measured backscatter coefficients with structural features of the floes under consideration. For example, principal features of the ice which determine the backscatter are the degree of surface roughness at the snow/ice (or air/ice interface in the absence of a snow layer), and the effective complex permittivity of the ice near its top surface. However, other features can significantly affect the return [17], such as a slush layer at the snow/ice interface, which can arise from flooding of the ice surface due to the weight of a snow layer, which depresses the ice surface below sea level. We saw evidence that this flooding of the surface was sometimes due to the coalescing of the brine pockets, which makes the sea ice porous, so that sea water can percolate up through the ice. This percolation threshold of the ice was reached under the influence of a "warm" storm, or a warm upwelling event. While volume scattering from brine and air inclusions within the sea ice or from the snow layer can affect the return, its influence is minimal compared with surface scattering, except at high incidence angles (close to grazing). The influence of volume scattering from inside the sea ice in the current situation is further reduced, though, since we were dealing primarily with first year, highly saline ice which is difficult to penetrate due to high attenuation.

We have only begun the analysis, yet can already see the pronounced effect of warming events on the backscatter. A central part of the cruise was to set up drift camps, where the ship was moored to a large floe in the pack, and allowed to simply drift with the pack. We were fortunate to obtain a five day time series of backscatter measurements, during which two distinct warming events occurred. At low incidence angles, such as 30 or 35 degrees from vertical, we see a good correlation between the backscatter coefficient and the temperature near the surface of the ice. One explanation for this is that as the temperature increases, the brine volume of the ice increases, which in turn increases the permittivity of the ice, thus increasing the backscatter. Other findings support this type of correlation. Current efforts are devoted to developing backscatter models to quantitatively analyze the time evolution of the data, and its relation to observed temperature profiles of the ice.

REFERENCES

[1] J. Addison, *Electrical properties of saline ice*, *J. Appl. Phys.*, 40:3105–3114, 1969.

[2] S.A. Arcone, A.J Gow, and S. McGrew, *Structure and dielectric properties at 4.8 and 9.5 GHz of saline ice*, *J. Geophys. Res.*, 91(C12):14281–14303, 1986.

[3] D.J. Bergman, *The dielectric constant of a composite material–A problem in classical physics*, *Phys. Rep. C*, 43:377–407, 1978.

[4] D.J. Bergman, *Exactly solvable microscopic geometries and rigorous bounds for the complex dielectric constant of a two-component composite material*, *Phys. Rev. Lett.*, 44:1285, 1980.

[5] D.J. Bergman, *Rigorous bounds for the complex dielectric constant of a two–component composite*, *Ann. Phys.*, 138:78, 1982.

[6] O. Bruno, *The effective conductivity of strongly heterogeneous composites*, *Proc. R. Soc. London A*, 433:353–381, 1991.

[7] O. Bruno, *Effective moduli of strongly heterogeneous composites*, In G. Bouchitté, G. Butazzo, and P. Suquet, editors, *Calculus of Variations, Homogenization and Continuum Mechanics*, pages 99–115, World Scientific Publishing Co., Singapore, 1994.

[8] E. Cherkaeva and K.M. Golden, *Inverse bounds on the brine volume of sea ice from complex permittivity data*, In preparation.

[9] G.F.N. Cox and W.F. Weeks, *Equations for determining the gas and brine volumes in sea-ice samples*, *J. Glaciology*, 29:306–316, 1983.

[10] G. Frankenstein and R. Garner, *Equations for determining the brine volume of sea ice from −0.5° to −22.9° C*, *J. Glaciology*, 6(48):943–944, 1967.

[11] K. Golden, *Bounds on the complex permittivity of a multicomponent material*, *J. Mech. Phys. Solids*, 34(4):333–358, 1986.

[12] K. Golden, *Bounds on the complex permittivity of sea ice*, *J. Geophys. Res. (Oceans)*, 100(C7):13,699–13,711, 1995.

[13] K. Golden and G. Papanicolaou, *Bounds for effective parameters of heterogeneous media by analytic continuation*, *Comm. Math. Phys.*, 90:473–491, 1983.

[14] K.M. Golden and S.F. Ackley, *Modeling of anisotropic electromagnetic reflection from sea ice*, *J. Geophys. Res.*, 86(C9):8107–8116, 1981.

[15] Z. Hashin and S. Shtrikman, *A variational approach to the theory of effective magnetic permeability of multiphase materials*, *J. Appl. Phys.*, 33:3125–3131, 1962.

[16] P. HOEKSTRA AND P. CAPILLINO, *Dielectric properties of sea and sodium chloride ice at UHF and microwave frequencies*, *J. Geophys. Res.*, 76:4922–4931, 1971.
[17] A.R. HOSSEINMOSTAFA, V.I. LYTLE, K.C. JEZEK, S.P. GOGINENI, S.F. ACKLEY, AND R.K. MOORE, *Comparison of radar backscatter from Antarctic and Arctic sea ice*, *J. Electromagnetic Appl.*, 9:421–438, 1995.
[18] V.I. LYTLE AND K.M. GOLDEN, *Microwave backscatter measurements from first year pack ice in the eastern Weddell Sea*, *Antarctic Journal of the U.S.*, 30:125–127, 1995.
[19] C. MÄTZLER AND U. WEGMÜLLER, *Dielectric properties of fresh-water ice at microwave frequencies*, *J. Phys. D: Appl. Phys.*, 20:1623–1630, 1987.
[20] G.W. MILTON, *Bounds on the complex dielectric constant of a composite material*, *Appl. Phys. Lett.*, 37:300–302, 1980.
[21] R. SAWICZ AND K. GOLDEN, *Bounds on the complex permittivity of matrix-particle composites*, *J. Appl. Phys.*, 78:7240–7246, 1995.
[22] R.A. SHUCHMAN AND R.G. ONSTOTT, *Remote sensing of the polar oceans*, In W. O. Smith, editor, *Polar Oceanography, Part A, Physical Science*, pages 123–169, Academic Press, New York, USA, 1990.
[23] A.H. SIHVOLA AND J.A. KONG, *Effective permittivity of dielectric mixtures*, *IEEE Trans. Geosci. Remote Sensing*, 26(4):420–429, 1988.
[24] A. STOGRYN, *An analysis of the tensor dielectric constant of sea ice at microwave frequencies*, *IEEE Trans. Geosci. Remote Sensing*, GE-25(2):147–158, 1985.
[25] A. STOGRYN AND G.J. DESARGANT, *The dielectric properties of brine in sea ice at microwave frequencies*, *IEEE Trans. Ant. Prop.*, AP-33(5):523–532, 1985.
[26] W.R. TINGA, A.G. VOSS, AND D.F. BLOSSEY, *Generalized approach to multiphase dielectric mixture theory*, *J. Appl. Phys.*, 44(9):3897–3902, 1973.
[27] M.R. VANT, R.O. RAMSEIER, AND V. MAKIOS, *The complex-dielectric constant of sea ice at frequencies in the range 0.1–40 GHz*, *J. Appl. Phys.*, 49(3):1264–1280, 1978.

ELECTRON IN TWO-DIMENSIONAL SYSTEM WITH POINT SCATTERERS AND MAGNETIC FIELD

SERGEY GREDESKUL*, MASHA ZUSMAN†, YSHAI AVISHAI‡, AND MARK YA. AZBEL§

Abstract. This paper is a survey of the electron spectral properties (eigenenergies and wave functions) in a two dimensional system containing point scatterers and subject to a perpendicular magnetic field. Point potentials scatter only s-waves and do not influence waves with higher orbital momentum. Therefore they lift the infinite degeneracy of the Landau levels only partially. As a result the spectrum can be divided into two parts: the set of discrete Landau levels and the set of intervals between these levels. The states on the Landau levels exist in a strong enough magnetic field (the flux per a scatterer has to be larger than a flux quantum). They are regular functions of the spatial coordinates and vanish at the sites where the point scatterers are located. A new approach, based on the theory of entire functions, is proposed for studying of these states, and some of them are explicitly constructed.
States outside the Landau levels exist for an arbitrary magnetic field and have logarithmic singularities at all points where the scatterers are placed. In the ordered case (identical scatterers, placed on the sites of a square lattice) and for some rational values of a magnetic field, dispersion laws are numerically calculated and the Hofstadter-type butterfly is constructed. It is shown that the dispersive subbands in a square lattice of identical point scatterers in the strong field limit are described by the Harper equation. The problem of electron localization in such a system with one dimensional disorder reduces in the strong field limit to the random Harper equation. An explicit formula describing the fractal structure of the localization length is obtained. This structure is influenced by the amplitudes of the Bloch states in the corresponding ordered system.

1. Introduction. Three decades ago low-dimensional conducting systems were often considered as some exotic and in a sense academic subjects of investigations. But recent interest in these systems from a purely scientific point of view, as well as from its application aspects, mainly modern microelectronics, — stimulated a significant progress in their fabrication [56], [68] which in its turn led to the discovery of a variety of remarkable new properties of such systems.

Two-dimensional (2D) conducting systems can be realized as both natural and artificial objects. Indeed, thin films, surfaces or intersurfaces can be often considered as 2D systems. But the most popular realization of 2D conducting system is an inversion layer, which can be created near the interface between semiconductor and dielectric (for example, between semiconductor Si and dielectric SiO_2), or near the interface between two

* Department of Physics, Ben Gurion University of the Negev, PO Box 653, 84105 Beer-Sheva, Israel.
† Department of Physics, Ben Gurion University of the Negev, PO Box 653, 84105 Beer-Sheva, Israel.
‡ Department of Physics, Ben Gurion University of the Negev, PO Box 653, 84105 Beer-Sheva, Israel.
§ Raymond and Beverly Sackler School of Physics and Astronomy, Tel-Aviv University, 69978 Ramat Gan, Israel.